In-Depth Study of Ambipolar Charge-Transport Regime through External Triggers and Gas Sensing

Sujithkumar Ganesh Moorthy, Adehouyi Apoubou, Seydou Ouedraogo, Lucas Vachey, Mabinty Bayo-Bangoura, Marcel Bouvet

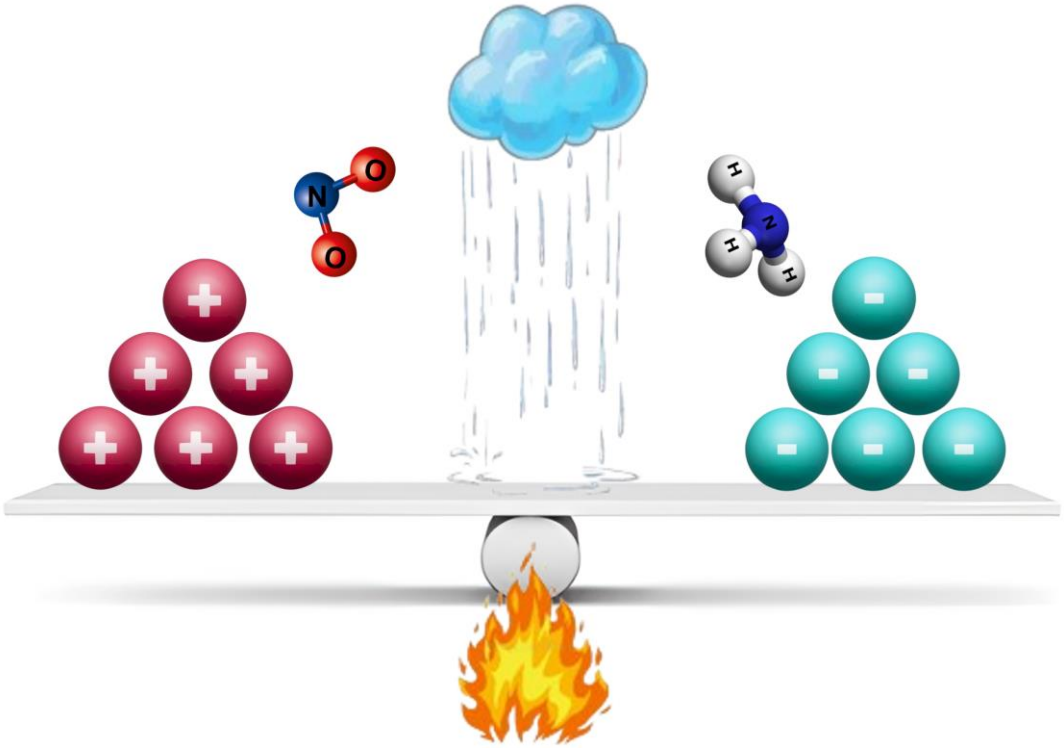
N
O
O
H
N
H
H

In-depth study of ambipolar charge transport regime through external triggers and gas sensing

Sujithkumar Ganesh Moorthy[†], Adehouyi Apoubou[‡], Seydou Ouedraogo[‡, §], Lucas Vachey[†], Mabinty Bayo-Bangoura[‡]*, Marcel Bouvet[†] *

*Corresponding authors: mabintybayo@yahoo.fr; marcel.bouvet@u-bourgogne.fr

[†]*Institut de Chimie Moléculaire de l'Université de Bourgogne (ICMUB), Université de Bourgogne, UMR CNRS 6302, 9 avenue A. Savary, F-21078 Dijon, France,*

[‡]*Laboratoire de Chimie Moléculaire et de Matériaux, Université Joseph Ki-Zerbo, 03 BP 7021 Ouagadougou 03, Burkina Faso*

[§]*Institut des Sciences et de Technologie de l'Ecole Normale Supérieure, 01BP 1757 Ouagadougou 01, Burkina Faso.*

Keywords: Organic heterojunction, octafluorophthalocyanine, lutetium bisphthalocyanine, ambipolar device, polarity inversion, ammonia, nitrogen dioxide.

Abstract

Ambipolar devices is a hot topic in research's table due to its unique advantage in reducing the size of the electrical system and enhancing its efficiency. Here, we report a bilayer heterojunction device constructed using octafluoro-vanadyl-phthalocyanine (VOF_8Pc) and lutetium bisphthalocyanine ($LuPc_2$), which exhibits both p- and n-type behaviors under oxidizing (NO_2 and O_3) and reducing gas (NH_3) species depending on the humidity level and temperature variations. The initial polarity of the device is identified as n-type by measuring a current decrease under oxygen exposure. Most interestingly, we were capable to observe the zero state (no response) where both opposite charge carriers fighting for the majority to dominate the electrical properties of the device when it goes from n- to p-type or vice versa. The inversion in nature of majority charge carrier densities in this ambipolar device was achieved by optimizing the external trigger. The unique property of controllable polarity inversion in $VOF_8Pc/LuPc_2$-based bilayer heterojunction device makes it as a most effective ambipolar device for real world application.

Introduction

The innovation in molecular semiconductors have pushed them as pivotal materials in new electrical applications, due to their tunable electronic properties and potential for low-cost, flexible device applications.[1-3] Characterized by their conjugated molecular structures, these organic compounds are electrically tunable and have the ability to undergo extensive molecular

engineering.[4-6] This versatility is crucial for developing the next-generation of electronic devices that require high performance and adaptability.

In today's advanced world, there is a high demand for miniature devices like wearable systems,[7] particularly a device performing multiple functions. This need has brought special attention to ambipolar devices.[8] In the past few decades, researchers globally have focused on developing materials possessing nearly equal densities of mobile charge carriers in molecular materials, which can be used to create bipolar (both p- and n-type) devices known as ambipolar devices.[9-11] These types of devices can work in both polarities upon utilizing external trigger to switch the states. Heterojunction-based ambipolar transistors controlled by an electrical trigger are a representative example of such ambipolar devices.[12] Till now, three main external triggers for ambipolar sensing devices have been reported in the literature: electrical, optical and humidity variations.[13-14]

Electrical trigger is often used in ambipolar organic field-effect transistors in the form of applying potential difference across the gate terminal of the transistor. For instance, in 1990, J. Simon et al. reported the first-ever molecular semiconductor-based transistor exhibiting both p- and n-type behaviors using lutetium bisphthalocyanine ($LuPc_2$), depending on the gate voltage direction and surrounding atmosphere.[15] Under vacuum, the device displayed n-type behaviors with a positive gate voltage, while no transistor effect was observed with a negative gate voltage. Conversely, in ambient conditions, the same device exhibited p-type behaviors with a negative gate voltage, while no transistor effect was observed with a positive gate voltage. Later in 2011, Dodabalapur et al, reported the first ever chemical sensor based on an ambipolar transistor, consisting of two superposed semiconducting layers: zinc oxide (ZnO) an n-type semiconductor, covered by pentacene as a p-type semiconductor. In the p-channel accumulation mode ($V_{GS} < V_{DS} < 0$), a decrease in current was observed under ethanol vapors due to positive charges being trapped in the pentacene layer. Conversely, in the n-channel linear regime ($V_{GS} < V_{DS} < 0$), an increase in current was observed. Notably, in the n-channel accumulation regime ($V_{GS} > V_{DS} > 0$), the device was insensitive to ethanol.[16]

In 2013, M. Bouvet et al. introduced and patented a new type of heterojunction device consisting of poor conducting sublayer covered by highly conducting molecular material as a top layer ($LuPc_2$)[17] (**Scheme 1**). With this device architecture, we demonstrated different types of gas sensors.[18-19] $LuPc_2$ is a stable radical that can be easily oxidized and reduced.[20] Moreover, it possesses huge densities of > 0 and < 0 charge carriers near equilibrium, which opens the gateway for the sublayer to choose the polarity of the device when it engages in heterojunction devices.[21]

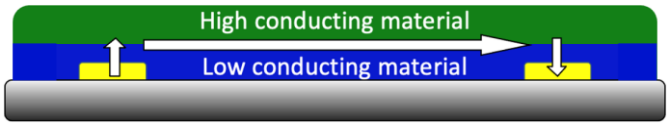

Scheme 1. Schematic view of double layer heterojunction device. Arrows represent the charge transport pathway.

In our previous publications, we demonstrated ambipolar charge transport in organic heterojunction devices utilizing both optical and humidity variations as external triggers.[9, 22] By modulating the degree of halogenation in metallophthalocyanines, we developed a series of bilayer semiconductor devices that consist of both unsubstituted and fluorinated copper phthalocyanines, Cu(F_nPc) (n = 0, 8, 16), as sublayers, with $LuPc_2$ serving as the top layer.[22] Our findings revealed distinct behaviors under varying conditions: CuPc displayed p-type characteristics when exposed to ammonia, while $CuF_{16}Pc$ exhibited n-type behaviors. Notably, CuF_8Pc showed p-type characteristics in the dark and n-type under red LED illumination. Additionally, we investigated octachloro-phthalocyanine complexes with various metal centers (Cu, Zn, and Co). Within this series, we achieved ambipolar charge transport in a $ZnCl_8Pc/LuPc_2$ heterojunction device using humidity as an external trigger. This device exhibited p-type behavior under ammonia exposure at high humidity levels (50%) and n-type behavior at lower humidity levels (30%).[9]

This observed inversion in nature of majority charge carriers upon light exposure and humidity variations can be attributed to the detrapping effect. Oxygen and water molecules can act as a trap for mobile negative charge carriers. It is well known that the light can facilitate oxygen desorption. Hence upon illumination and at lower humidity levels, previously trapped charges are set free and it makes the minority (charge carriers) to became the majority, resulting in polarity inversion in the electrical conductivity of the device. This phenomenon underscores how a minimal external trigger can alter the nature of majority charge carriers in molecular semiconductor heterojunction devices, facilitated by the near-equilibrium state between charge carrier densities in the sensing layers.

In this manuscript, we synthesized the octafluoro-vanadyl-phthalocyanine complex (**Scheme 2a**) and engaged it with $LuPc_2$ (**Scheme 2b**) in organic-organic heterojunction device. The electrical and sensing properties of the $VOF_8Pc/LuPc_2$ device were thoroughly investigated under various conditions. Particularly, we delved into the mechanisms by which external triggers influence the behavior of the system, and highlights the control over the nature of majority charge carriers (polarity switching) as much as possible. Additionally, this is a first report utilizing a temperature variation as a new type of external trigger to inverse the nature of majority charge carrier density in organic heterojunction devices.

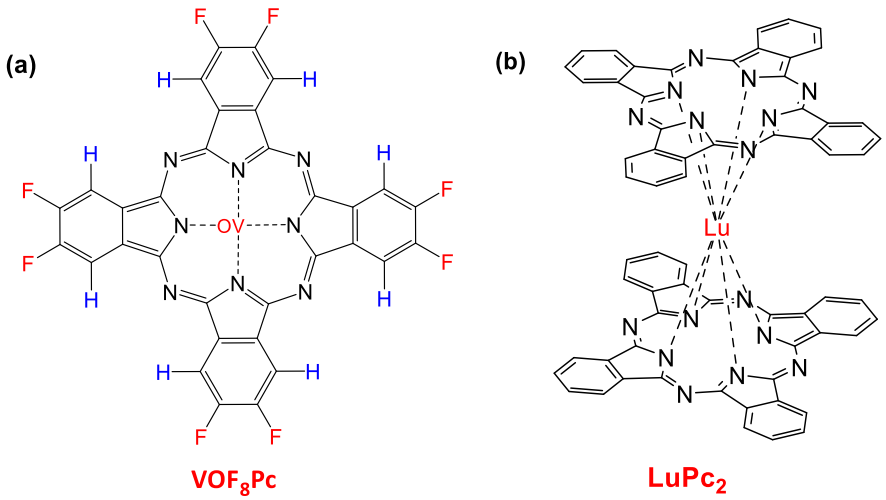

Scheme 2. Chemical structure of octafluoro-vanadyl-phthalocyanine (VOF_8Pc) (a) and lutetium bisphthalocyanine ($LuPc_2$) (b).

The heterojunction device was characterized by UV-Vis absorption and Raman spectroscopies. Additionally, current-voltage (I-V) measurements were conducted under different experimental conditions and charge transport properties were explored by Impedance spectroscopy measurements. For better understanding the charge transport properties, we conducted the sensing experiment in ppm range for NH_3 and ppb range for NO_2 and O_3

Experimental methods

Materials

VOF_8Pc was synthesized from 4,5-difluorophthalonitrile by reacting at 200 °C during 2.5 h, in a glass tube, with vanadyl diacetate $VO(OAc)_2$, modified from the initial reported synthesis by T. Basova using VCl_3 as vanadium salt.[23] The obtained solid was washed with distilled water, then ethyl alcohol, each 3 times, with 15 min in an ultrasonic bath and 20 min centrifugation at 3500 rpm. Solid was then dried at 100 °C under primary vacuum for 2 h. $LuPc_2$ was synthesized from o-phthalonitrile and lutetium triacetate by heating at 300 °C without any solvent for 3 h, according to previously reported method.[20]

Device fabrication

The fabrication of our heterojunction device began with the sequential thermal evaporation of VOF_8Pc and $LuPc_2$ on Indium Tin Oxide (ITO) interdigitated electrodes (IDEs). These IDEs consisted of 16 pairs of ITO digits, each with a width and spacing of 75 µm, fabricated on a glass substrate using lithography techniques. Prior to deposition, the electrodes

underwent thorough cleaning with CH_2Cl_2 and EtOH through multiple stepwise ultrasonication cycles, each for 5 min, followed by drying in an oven at 100 °C for 1 hr.

Utilizing a German made UNIVEX 250 thermal evaporator (equipped with dual crucibles), a 50 nm-thick film of VOF_8Pc was initially deposited on the ITO IDEs, as controlled by a quartz crystal microbalance. The sublimation temperature ranged from 350 to 400 °C, with a deposition rate of ≈ 0.2 Å s^{-1}, preformed under secondary vacuum (ca. 7×10^{-7} mbar). Subsequently, $LuPc_2$ was deposited over VOF_8Pc as a top layer, without breaking the vacuum, utilizing another available crucible in the evaporator. The sublimation temperature range for $LuPc_2$ was recorded as 450 to 480 °C, and the deposition rate was maintained similar to that of VOF_8Pc. During deposition, a glass substrate was placed next to the IDE electrodes to get an identical bilayer heterostructure, to be used for optical and microstructural characterizations. To ensure consistency and reliability, three batches of the same device were prepared by repeating the deposition process with an interval period of approximately one month.

Electrical measurements

All electrical measurements were conducted using a Keithley 6517B electrometer. The UNIVEX 250 thermal evaporator was equipped with the capability to conduct electrical measurements under secondary vacuum conditions. This enabled us to measure the current values, sequentially, during the deposition process of both the sublayer and top layer over the electrodes, starting from the empty IDE up to the formation of the bilayer heterojunction. The measurements were continued throughout the venting process. To investigate the effect of oxygen on the device, we cyclically pumped and vented the chamber at specified intervals using the primary vacuum pump of the UNIVEX 250 thermal evaporator and continuously measured the current change.

The Current-Voltage (I-V) measurements were recorded by applying a bias voltage ranging from -10 V to +10 V in steps of 0.1 V, under different conditions. In ordered to avoid any polarization effect, the I-V measurements were started and ended at 0 V. Impedance measurements were carried out using a Solartron SI 1260 impedance analyzer, applying a fixed AC oscillation amplitude of 0.2 V in the frequency range of 10 Hz to 10 MHz and a DC bias ranging from 0 V to 10 V. Obtained data were treated using Ametek's Zview software.

Thin film characterization

The optical absorption properties of the materials and bilayer device were measured by Cary 50 (Varian) UV-vis spectrophotometer, between 300 and 1000 nm and Raman spectral measurement was conducted on the samples using a Renishaw inVia microscope at an

excitation wavelength of 473 nm with 1% of 12 mW laser power, under 50x magnification. Multiple datasets were acquired for both materials and device to derive an average representative spectrum for all normalized Raman spectra.

Sensing experiments

The detailed experimental setup utilized for electrical and gas sensing measurements under different conditions is depicted in **Scheme 3**. It comprises fluidic circuits interconnected with commercial cylinders containing synthetic air, ammonia gas (with a concentration of 1000 ppm mol/mol), nitrogen dioxide (with a concentration of 10 ppm mol/mol) purchased from Air Liquide France and with an ozone generator (O_3 41M Environment S.A., France).

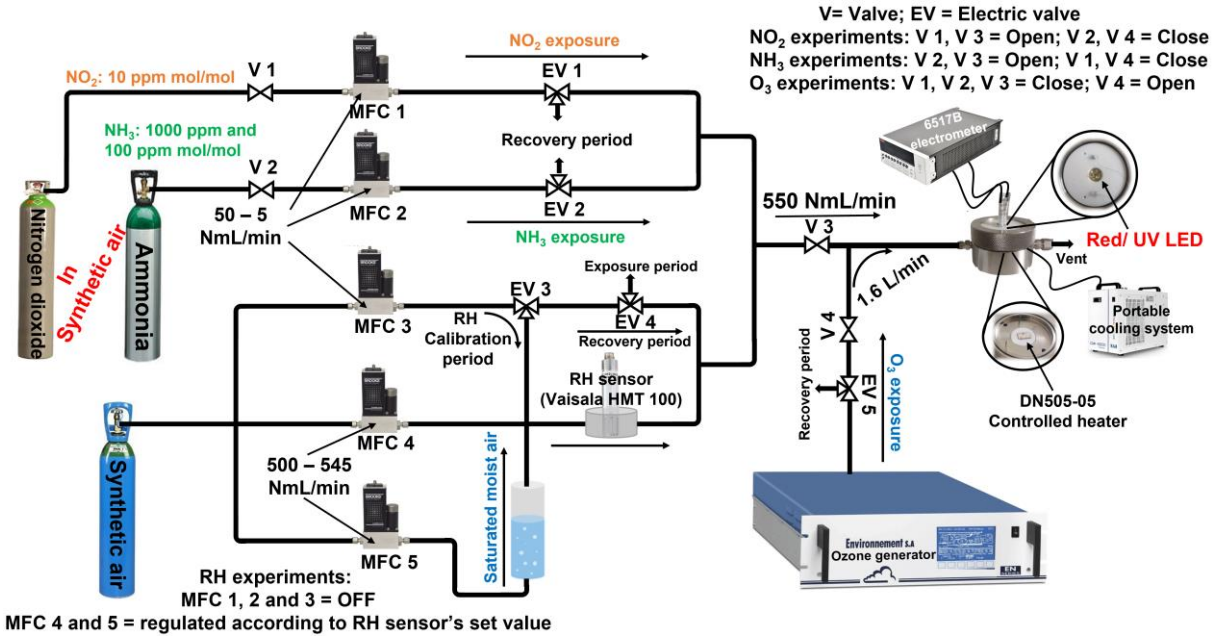

Scheme 3. Illustration of homemade device testing workstation integrating different gas sources, fluidic circuits, mass flow controllers, electronic valves, water column, humidity sensor, ozone generator, electrometer, and test chamber equipped with a controlled heater, a cooling system and red LEDs.

The gas flow within the circuit is controlled as per our desired gas concentration and exposure/recovery time using various mass flow controllers (Brooks Instrument) and electric valves, respectively. Precise control over relative humidity is achieved with the help of a commercially available humidity sensor (HMT 100, Vaisala, Finland) interconnected with mass flow controllers. Both the mass flow controllers and humidity sensor are interfaced with a PID program, enabling the precise dilution of humidity saturated air from the water column with dry air to maintain a standardized relative humidity value. A small flow of target gas (ca. 5 to 50 NmL min^{-1}) was introduced into the previous flow to generate air with controlled gas

concentrations, in the range of 10 – 90 ppm and 100 – 900 ppb depending on the concentration in the NH_3/air and NO_2/air cylinders, respectively. Except for ozone experiments (total mass flow: 1.6 L min^{-1}), the total gas flow was kept constant throughout all the experiments (550 NmL min^{-1}).

All gas sensing experiments were carried out using homemade gas chamber (volume 8 cm^3), which is equipped with DN505-05 controlled heater positioned at the bottom, ensuring precise temperature regulation, while three red LEDs are strategically positioned 2 cm above the test sample, providing consistent illumination. Furthermore, the chamber is connected to a cooling system, facilitating rapid cooldown when necessary. The workstation was fully automated in which the gas concentration, humidity values, switching of the value, PID control, temperature regulation, light illumination and data transfer were controlled by homemade and customized software.

Results and discussion

UV-visible absorption and Raman diffusion spectroscopies

Both $LuPc_2$ and VOF_8Pc film, and the resulting bilayer heterostructure ($VOF_8Pc/LuPc_2$) were characterized using a UV-visible spectrophotometer across the wavelength range of 300 to 1000 nm. The superimposed spectra are presented in the **Figure 1**.

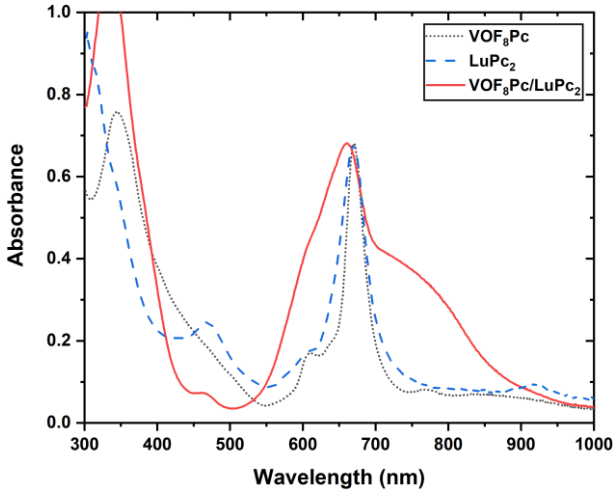

Figure 1. Absorption spectrum of $VOF_8Pc/LuPc_2$ bilayer heterostructure (red line) compared to the spectra of $LuPc_2$ (blue dash line) and VOF_8Pc (black dotted line) in THF solutions.

Both materials and heterostructure exhibit a typical Q-band, originating from the electron transition from the Highest Occupied Molecular Orbital (HOMO) to the Lowest Unoccupied Molecular Orbital (LUMO) ($\pi \rightarrow \pi^*$ transition).[24] In solution, both phthalocyanine complexes exhibit a main absorption peak at 668 nm. While the main peak of $LuPc_2$ remains consistent in the heterojunction film, the main peak of the sublayer broadens into a shoulder.

As previously reported by T. Basova,[23] the VOF_8Pc film exhibits a broad red-shifted Q-band. It can be correlate to J-aggregate formation, compared to its spectra in solution. Consequently, the main peak from the sublayer shifts entirely to around 750 nm and appears as a broad shoulder in the heterostructure film. It is quite particular in VOF_8Pc due to strongest interaction compared to ZnF_8Pc and CoF_8Pc. The shoulder at 608 nm in heterojunction film is significant for fluorinated compounds and similar shoulder was observed in $MF_{16}Pc$. The absorption band at 470 nm in heterostructure film is specifically associated with the Semi-Occupied Molecular Orbital (SOMO) of the $LuPc_2$ neutral radical, linked to the $e_1 \rightarrow a_2$ transition.[23, 25-26]

We compared the normalized Raman spectrum of heterostructure film with its counterparts (VOF_8Pc and $LuPc_2$) and observed that it is just a superimposition of chemical signatures of both layers as depicted from the stack view (**Figure S1**). We can conclude that no chemical transformation occurred during sublimation. The detailed information on Raman diffusion spectroscopy is given in supporting information and the data were compiled in **Table S1**.

Current measurement during deposition and oxygen effect

Throughout the deposition process of both layers onto the ITO-IDE substrate, we continuously monitored the flow of electric charges across the sample by applying a voltage of 3 V. This measurement was continued from the bare ITO-IDE to the formation of the heterojunction device, aiming to understand the electrical properties of the materials and their dependency on thickness on the ITO-IDE substrate (**Figure 2**).

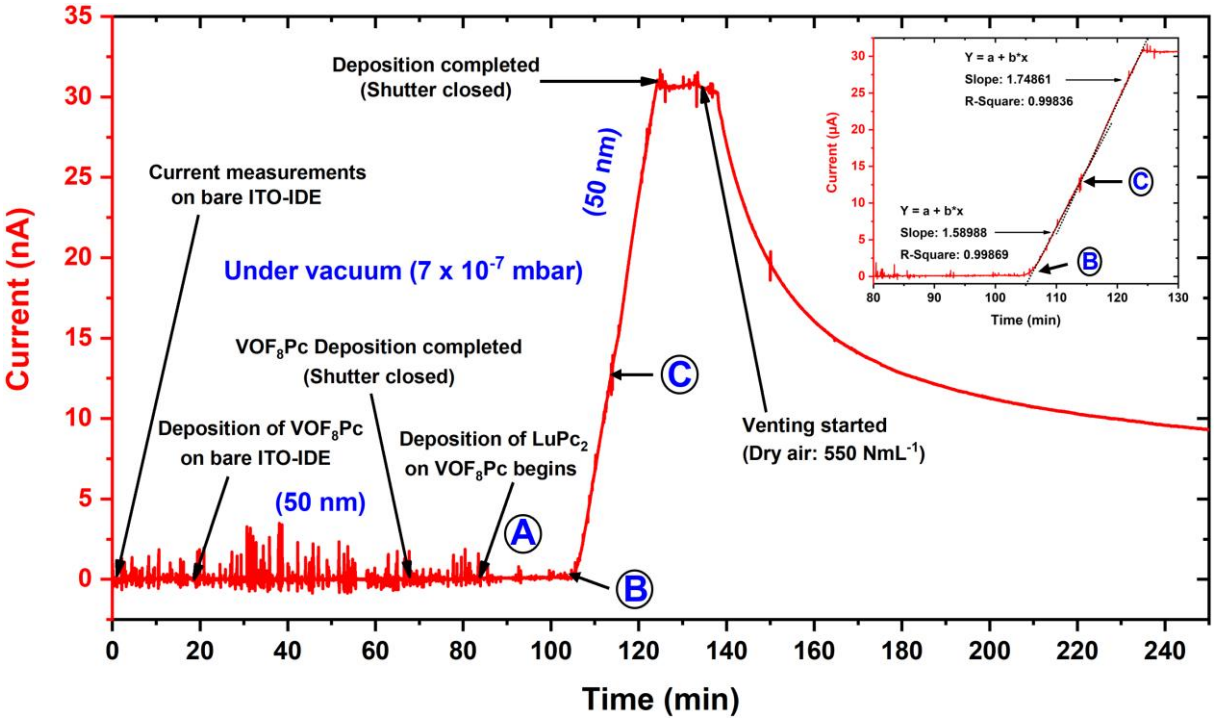

Figure 2. Current measurement during deposition process. The inset shows a zoomed view of the change in slope. The letters A, B, and C represent different singular points: A indicates a decrease in signal noise, B shows a sharp increase in current, and C denotes the change in slope.

The sublayer exhibits poor conductivity, as evidenced by very low and noisy signal throughout its deposition process, up to a thickness of 50 nm. However, upon initiation of the $LuPc_2$ deposition over the sublayer, a notable decrease in signal noise (i.e. from A), then a sharp increase in current is observed (i.e. in B). This increase follows a linear trend during ca. 20 min of $LuPc_2$ deposition, reaching thickness around 150 to 240 Å, indicating the establishment of a conducting channel. Subsequently, above ca. 250 Å, there is a change in i(t) slope (i.e. in C phase), suggesting total surface coverage by $LuPc_2$, which continued until the shutter closed at 500 Å. A zoom was added as inset in **Figure 2**. for better visibility of the change in slope.

Oxygen effect

After the deposition process, the vacuum chamber of the thermal evaporator was vented with dry air to investigate the solely effect of oxygen without interference of humidity on the electrical properties of the resulting device. Subsequently, the current exhibited an exponential decay upon exposure to oxygen, consistent with the n-type behavior of the device, since oxygen neutralizes negative charge carriers. To delve into this effect, we conducted cyclically pumping and venting of the chamber while continuously measuring the current change. Notably, during the pumping phase, the heterojunction sensor demonstrated a positive response, indicative of increased conductivity, whereas a decrease in current was observed during the venting period. This experimental observation provides further confirmation of the n-type nature of the device (**Figure 3**).

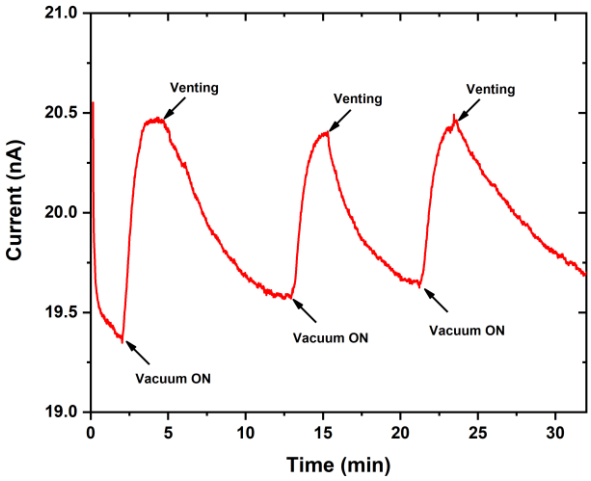

Figure 3. Effect of oxygen on $VOF_8Pc/LuPc_2$ heterojunction device.

Electrical properties of the device under different conditions.

To explore the impact of diverse atmospheric surroundings on the electrical characteristics of the heterojunction device, we performed I-V measurements by applying a potential difference across the device, varying from -10 V to +10 V, under different conditions. Initially, we conducted the I-V experiments under secondary vacuum (ca. 7 x 10^{-7} mbar), followed by exposure to 45% Relative Humidity (RH), NH_3 (90 ppm), NO_2 (900 ppm), and red-light illumination and under heating condition (80 °C) (**Figure 4**).

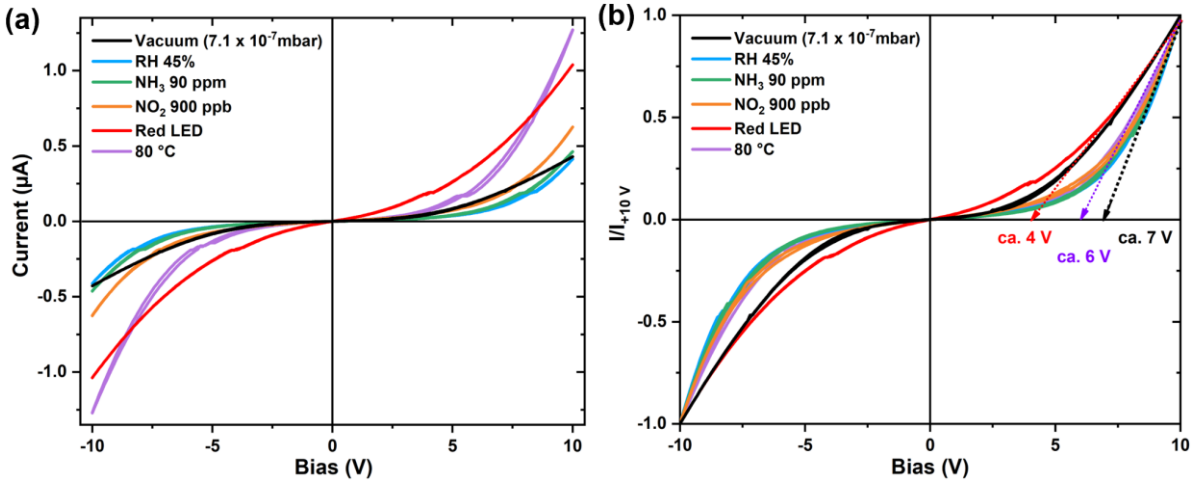

Figure 4. I-V characteristics of the heterojunction device under different atmospheric conditions (a) and its normalized view (b).

It is noteworthy that under all conditions, the device exhibits non-linear and symmetrical I-V curve. This non-linearity is characteristic of bilayer heterojunction devices composed of materials with different work functions, originating from the accumulation of mobile charges at the interface [21, 27]. However, the degree of non-linearity is intricately linked to the formation of the interface between the organic layers and to the charge transport resistance in both layers [28]. Taking the advantage of non-linearity in I-V curves, we can estimate an apparent energy barrier by drawing tangents at higher voltage on the I-V curves and extrapolating them to the x-axis, providing insights into the threshold voltage (U_{th}). I-V curves allow comparing current values in the different conditions (**Figure 4a**). The normalized I-V characteristics, obtained by plotting I (V)/$I_{+10\ V}$ as a function of bias offer a clear perspective on realizing the apparent energy barrier of the device under various conditions (**Figure 4b**).

In current scenario, the resistivity of the sublayer is very high compared to this of $LuPc_2$, resulting in low current (ca. 0.4 µA at +10 V) and high U_{th} values (7 V) under ambient conditions. When exposed to NH_3 and NO_2, the current at +10 V increases to ca. 0.45 µA and 0.6 µA, respectively. However, these gases do not affect the apparent energy barrier of the heterojunction device. Surprisingly, under secondary vacuum (ca. 7 x 10^{-7} mbar) and red-light

illumination the U_{th} values roughly halved compared to other conditions. However, the current at +10 V under red-light illumination is ca. 1 µA, significantly higher than the current under secondary vacuum (ca. 0.4 µA), although they shared similar U_{th} values. Interestingly, the current value at +10 V under vacuum coincides that under ambient conditions but with a lower U_{th} value (ca. 4 V). Finally, when the device temperature is increased to 80 °C, the current at +10 V rises to ca. 1.3 µA, and the apparent energy barrier is modified to ca. 6 V. These values are summarized in the **Table S2** for better understanding.

To gain insights into the electrical properties of the heterojunction device and the charge transport regime at the interface, impedance spectroscopy measurements were conducted. A fixed amplitude of 0.2 V AC signal was applied, covering a wide range of frequencies from 10 Hz to 10 MHz, under various DC bias conditions (ranging from 0 to 10 V). All the impedance spectroscopy measurements were conducted in ambient conditions. The impedance spectroscopy results, as depicted through Nyquist plots showing the imaginary part versus the real part of the impedance, offer valuable insights into the distinct charge transport characteristics observed at the interface and within the bulk of the bilayer heterojunction device (**Figure 5**). These plots reveal two distinct depressed semicircles, which is a characteristic feature of typical bilayer heterojunction devices.[21] Detailed explanation and fitting of Nyquist plots and deduced parameters (resistances, alpha and capacitances) using **equations S1** and **S2** characterizing bulk and interface (**Figure S2**) are given in supporting information.

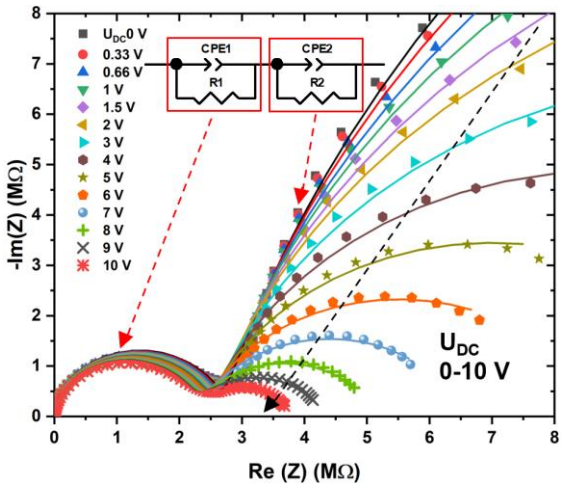

Figure 5. Nyquist plots of VOF_8Pc-based heterojunction device measured at fixed AC (0.2 V) superimposed by variable DC voltage in the range of 0-10 V. The inset shows the equivalent circuit selected for fitting Nyquist plots.

Exploring the ambipolarity of the bilayer device through different gas species

Initially, the as-prepared sample was investigated under 90 ppm of NH_3, a weak electron donating gas species, for time periods of 10 min exposure followed by 30 min recovery under

clean air in ambient conditions (18 °C and 45% RH). The device exhibited current increase under NH_3 exposure and decrease during recovery period, which is characteristic of an n-type device (**Figure 6a**). The relative response (RR), defined as the current variation under NH_3 divided by the current in air, was ca. 19.5%. Furthermore, it confirms the measurements recorded during oxygen exposure, when the current decreased upon air entry in the vacuum chamber.

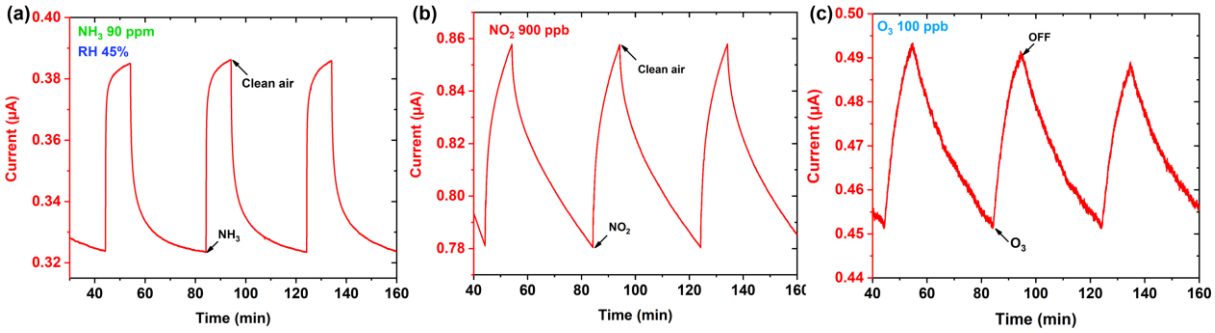

Figure 6. Response curve of $VOF_8Pc/LuPc_2$ heterojunction sensor, under successive exposures to 90 ppm NH_3 (a), 900 ppb of NO_2 (b) and 100 ppb of O_3 (c) for 10 min. This was followed by a dynamic recovery (under clean air) for NH_3 and NO_2, and a static recovery (without any flow) for O_3, each lasting 30 min at 45% RH and room temperature (18 – 19 °C).

However, under the same experimental conditions, upon exposure to 900 ppb of NO_2 and 100 ppb of O_3, both strong oxidizing species, a current increase was also observed, indicating a p-type behavior (**Figure 6b, c**). This inversion of polarity from n-type under NH_3 to p-type under oxidizing species means that the density of negative charge carriers (electrons) and positive charge carriers (holes) were almost at the equilibrium in the device in air. Even though it is very unusual, a few examples have already been reported by Y. Chen, with phthalocyanine-based resistors and field-effect transistors.[2, 11, 29] These devices are known as ambipolar devices.

The term ambipolarity can be explained by imagining a physical balance that owns infinite unbalance positions, but only one equilibrium state. In electrical device, this equilibrium can be achieved if the conductivities bore by both opposite charges were exactly equal. However, in real world, it is almost impossible to attain such an equilibrium state due to its highly unstable nature, but it is possible to attain near equilibrium state in organic materials, with the help of chemical engineering. To achieve the ambipolarity charge transport regime in electrical devices, we have to optimize the electrons (e^-) and holes (h^+) densities in the molecular semiconducting material near to the equilibrium. Actually, considering a possible difference in mobilities of electrons and holes, the product between the density of free charge carriers by their mobility has to be considered. If the currents bore by each type of charges in the organic

heterojunction devices are very near to the equilibrium, even a small external trigger can inverse the nature of majority charge carriers and a possibility to observe such an effect occurs. Such ambipolar devices are expected to be highly sensitive. Even a specific interaction with environment can highly influence the charge transport regime in such devices. To further understand the ambipolar behavior, we need an in-depth and careful consideration of the effects caused by some external parameters like humidity and temperature.

In-depth exploration of external triggers on ambipolar device

Light and temperature effects

Initially, the heterojunction device was tested under 1 min exposure to 20 ppm NH_3, followed by 4 min recovery under clean air, at 45% RH, both in dark and under red light from red LEDs (**Figure 7a**). As expected in organic electronics, a current increase was observed upon illumination, by slightly less than a factor of 2. Interestingly, the response to NH_3 increases under illumination. The device exhibited not only an increase in current variation under NH_3, from ca. 0.01 µA in the dark to ca. 0.05 µA under illumination, but also an increase in relative response (RR %) from 3.5% in the dark to 7% under illumination. Remarkably, under light exposure, both ΔI and RR of the heterojunction device increased, by ca. 5 and 2 times, respectively, compared to the values observed in dark condition.

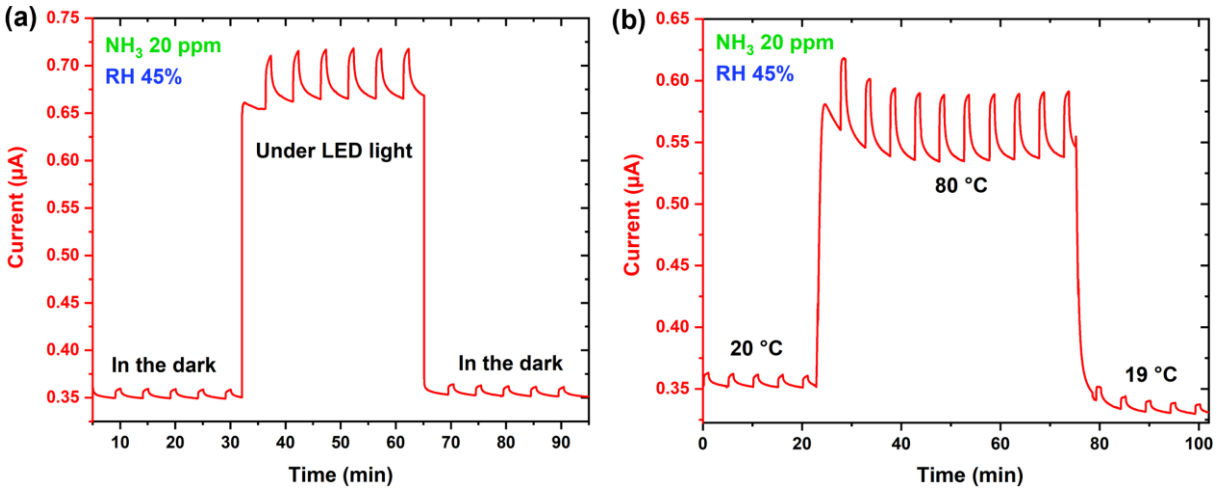

Figure 7. Response curve of $VOF_8Pc/LuPc_2$ heterojunction sensor, under successive exposures to 20 ppm NH_3 under different conditions: in the dark and under light (a), as well as in room temperature and 80 °C (b) at 45% RH.

Surprisingly, when the device was subjected to a temperature of 80 °C in a dark environment, it displayed a higher response compared to that at room temperature (19–20 °C) and even higher than under light exposure (**Figure 7b**). The RR increased to ca. 10.5%, roughly 5 times higher than in ambient conditions and 1.5 times higher than under light exposure.

However, the current shift was higher under light exposure (ca. 0.3 µA) compared to that at 80 °C (ca. 0.2 µA). It is well known that the RR values of conductometric sensors can be influenced by changes in temperature or light exposure, because of the induced mobile charges, oxygen desorption and accelerated adsorption/desorption kinetics.[30] However, upon closer inspection, differences in sorption kinetics can be observed between light exposure and heating conditions. When the lights are switched on and off, there is a sharp increase and decrease in current with a stable baseline. In contrary, under heating condition, there is an initial sharp increase in current, due to the activation energy of materials conductivity, followed by a decline in baseline current for the first few exposure/recovery cycles, after which it stabilized. This effect is directly linked to the desorption of water molecules from the organic layers, which influences the conductivity of the device (vide infra). However, after a few minutes, the baseline current becomes stable indicating the equilibrium state of the sensing material in terms of water contain.

To understand the solely effect of temperature on the heterojunction device, we conducted the same experiment on a freshly prepared sample under rather dry conditions (10% RH) across a wide temperature range, from 20 °C to 80 °C (**Figure 8a**).

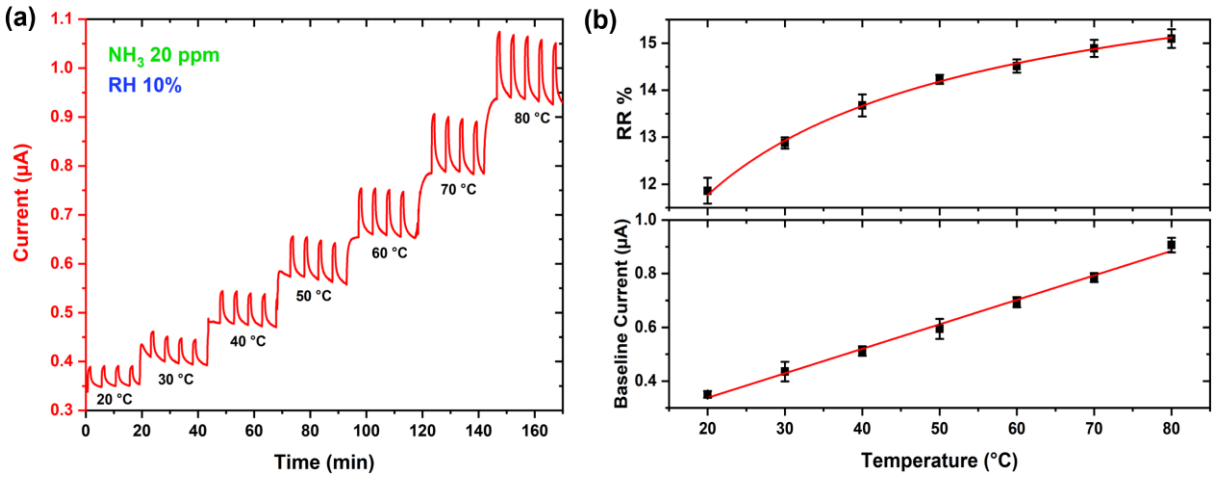

Figure 8. Response curve of $VOF_8Pc/LuPc_2$ heterojunction sensor, under successive exposures to 20 ppm NH_3 in a wide temperature range, from 20 °C to 80 °C in rather dry experimental condition (10% RH) (a). The variation in relative response and baseline current as a function of temperature (b).

Interestingly, we observed a similar decline in baseline current as we did previously at 80 °C, but this time it occurred at 30 °C and still slightly at 40 and 50 °C. It is apparent that the device attained more easily the equilibrium state at these temperatures, as a result of its initial dry state and the rather dry experimental conditions (10% RH). At 20 °C, in this rather dry environment, the device exhibited superior RR values (ca. 12%) compared to those in a humid atmosphere (RR 3.5% at RH 45%). This can be considered as surprising, since often it is the

reverse, the response to NH_3 increases when RH value increase, as a result of a higher affinity for NH_3 when sensing material is already covered by adsorbed water molecules.[31-32] However, an opposite factor can take place. Indeed, the surface density of available adsorption sites is higher for NH_3 molecules when less water molecules are adsorbed.[32] The baseline current increased linearly with temperature, while RR values increased exponentially (**Figure 8b**). Globally, these experiments confirm that the device exhibits higher n-type nature towards electron donating gas species in rather dry experimental conditions.

Humidity effect on the nature of majority charge carriers

In the realm of organic electronics and conductometric sensors, humidity represents a significant environmental factor that can substantially affect the electrical properties of devices. To explore the effect of humidity changes on the sensitivity towards NH_3 of the bilayer heterojunction device, we subjected a as prepared sample to NH_3 experiments. The experiments involved stepwise increasing of the humidity level from 20% to 80% and then monotonically decreasing to 20%, all conducted for 30 min at each RH values, while maintaining a constant temperature (20 °C) (**Figure S3**).

Remarkably, during RH increasing phase, the device maintained a stable baseline current with minimal sensitivity to humidity changes and displaying n-type behavior towards NH_3 across humidity levels from 20% to 60% RH. Fascinatingly, the n-type behavior of the bilayer device began to diminish, eventually transitioning to a p-type device at 80% RH and exhibiting a distinct negative response (current decrease) towards NH_3. Subsequently, the device stabilized into a consistent p-type behavior, even when same RH back to 20%.

In our previous study, we explored the properties of a $CuF_8Pc/LuPc_2$ based sensor, which demonstrated an ambipolar characteristic.[33] Specifically, the sensor exhibited a p-type behavior in low humidity value (30%) and switched to n-type upon exposed to higher humidity (70%). This remarkable behavior is due to the optimized degree of fluorination of CuF_8Pc compared to CuPc (pure p-type) and $CuF_{16}Pc$ (pure n-type), resulting in a balanced density of e^- and h^+ near equilibrium. Moreover, water molecules can trap the majority (positive) charge carrier in the sensing layer when the humidity increases. This process enables the density of negative charge carriers to surpass that of positive charge carriers, leading to the observed ambipolar behavior.

Remarkably, the $CuF_8Pc/LuPc_2$-based device transforms from p- to n-type, while VOF_8Pc-based device exhibits n-type behavior at the beginning and transformed to p-type upon humidity as external trigger. Changing the metal center from Cu^{2+} to VO^{2+} induces modification in the organization in the solid-state and the intermolecular interactions, due to the dipole-dipole

interactions that introduce a small shift in the frontier molecular orbitals of the MF_8Pc macrocycle, but significantly impact the nature of majority charge carriers within the devices. This effect can be also correlate with the different oxidation states and electronegativity of the metal center, as reported with metalated octachloro phthalocyanine-based heterojunctions.[26] In the current scenario, the formal oxidation state of V in VOF_8Pc is +4, the vanadyl is likely to be the dication VO^{2+}, which has higher electronegativity than Cu^{2+}, so induces a higher stabilization of electrons of the phthalocyanine macrocycle. This is the reason why in ambient conditions VOF_8Pc leads to a n-type device, while CuF_8Pc leads to a p-type device, the injection of electrons from the Fermi level of electrodes into the lowest unoccupied molecular orbital (LUMO) of VOF_8Pc becomes feasible, contrarily to what we observe with the copper complex.

To confirm the p-type behavior of the device, we subjected the same device, previously subjected to higher humidity levels, to 90 ppm NH_3 for an extended exposure/recovery cycle of 10 min/30 min in ambient conditions (19 °C and 45% RH). Remarkably, throughout numerous cycles, the device consistently maintained a stable p-type response over long exposure and recovery experiment (**Figure S4**). After exposure to higher humidity levels, the initially n-type device underwent a complete transformation into a stable p-type device. This transformation persisted even under ambient conditions, with the device exhibiting an RR of ca. -25%. Interestingly, the shapes of the response curves associated with adsorption and desorption phases present different profile in p-type state of the device, while comparing it to that of n-type state. When the heterojunction device was in n-type state, a continuous increase in current was observed throughout the exposure period, while in p-type state, a sharp current decrease followed by a plateau is observed. This difference in adsorption kinetics implies that in the n-type state, NH_3 molecules diffuse within the volume of the device and accesses additional sites within the bulk. On the other hand, in p-type state of the device, after adsorption NH_3 molecules can neutralize positive charge carriers in the $LuPc_2$ layer, and do not diffuse anymore. After a long exposure at high humidity, limited adsorption sites are available due to the presence of water molecules. As a result, sorption equilibrium of NH_3 is attained more rapidly during exposure period in the p-state.

Further investigation into the device's behavior involved testing it across a wide range of gas and humidity concentrations. Gas sensing experiments were conducted starting at 80% RH, decreasing incrementally in 20% steps down to RH level of 20%, with five exposure/recovery cycles at each NH_3 concentration (90, 60 and 30 ppm), at 20 °C (**Figure 9a**).

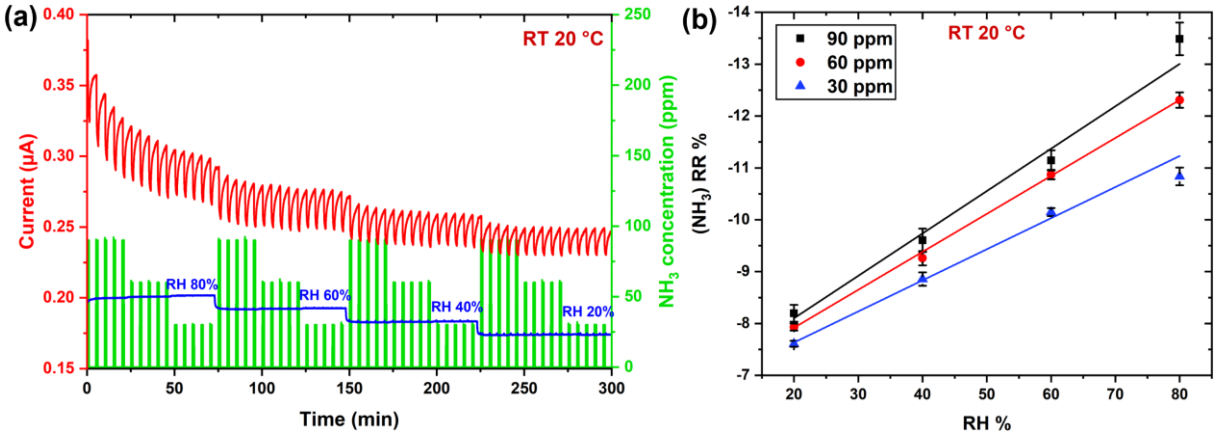

Figure 9. Response curve of $VOF_8Pc/LuPc_2$ heterojunction sensor under exposure to 90, 60, 30 ppm of NH_3 in humid air, in the range of 80 to 20% RH, during 1 min exposure followed by 4 min recovery, at 20 °C (a). The variation in relative response of the device as a function of RH (b).

Having conditioned the device at 80% RH, it consistently exhibited p-type behavior with minimal baseline drift. The absolute value of RR linearly increased with rising humidity levels, ranging from ca. 8.5% to 13.5% at 90 ppm NH_3 under RH values from 20% to 80%, respectively (**Figure 9b**). This suggests that increasing water content in the device promotes its p-type behavior. In other words, we can make the assumption that decreasing the water content in the device will continuously reduce the p-type behavior and eventually it will inverse its polarity to n-type. This assumption was proven by repeating the experiment at 80 °C, where the device demonstrated excellent n-type behavior, with RR of ca. 21% to 16% at 90 ppm across a wide range of humidity levels from 20% to 80%, respectively (**Figure 10**). Taking the advantage of the calibration curves (variation in RR vs NH_3 concentration **Figure S5**), we calculated the sensitivity and limit of detection (LOD) of the device using **equation S3** under different experimental conditions and polarities. The detailed explanation about LOD and the calculated values (**Table S3**) are given in supporting information.

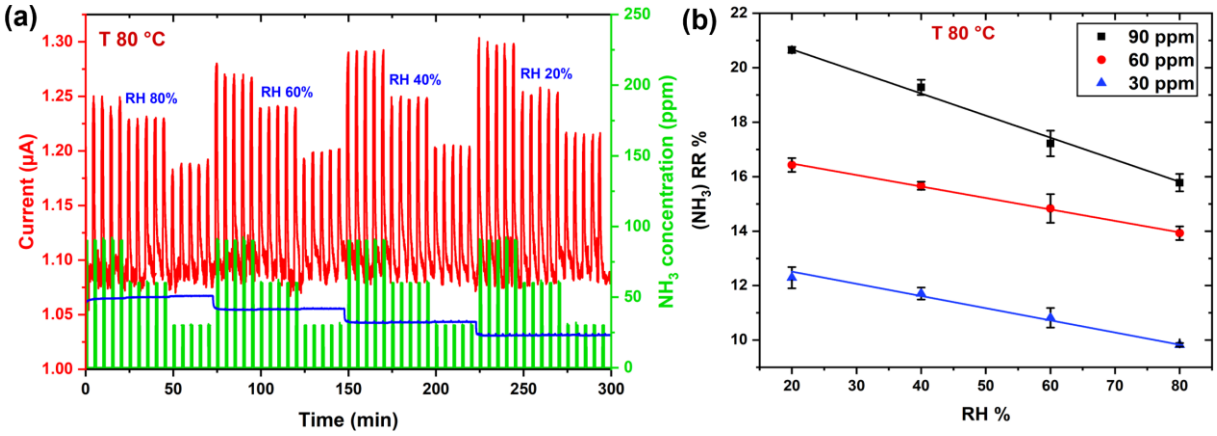

Figure 10. Response curve of $VOF_8Pc/LuPc_2$ heterojunction sensor under exposure to 90, 60, 30 ppm of NH_3 in humid air, in the range of 80 to 20% RH, during 1 min exposure followed by 4 min recovery, at 80 °C (a). The variation in relative response of the device as a function of RH (b).

It is mesmerizing to realize the possibility of operating a single device with good stability in both polarities, regardless of the natural environmental conditions. Interestingly, in its n-state the device's response to NH_3 decreased linearly with increasing humidity levels, further confirming the influence of water molecules on the response of the bilayer heterojunction device. It means that the absolute response (|RR|) to NH_3 decreases for n-state when RH value increases, but it increases for p-state. However, the adsorption of water molecules onto solid surfaces is a rather complex process influenced by humidity levels. At high humidity levels, water molecules condense on the sensor surface, forming a thin layer of liquid water.[34] This layer acts as a medium for target gases to dissolve into, enhancing their interaction with the surface of the device. This is particularly true for NH_3 that is highly soluble in water. However, at low humidity levels, water molecules form a hydrogen-bonded ice-like structured network on the surface, limiting the availability of active sites for gas adsorption.[35] In this case, water molecules compete with target gases for adsorption sites, reducing the sensor's response to the gases. Moreover, despite water molecules being typically electron donating species, they can also act as traps for the charges, affecting their mobility. This trapping effect can significantly influence the majority charge carriers' nature and determine the device's polarity. Besides adsorption, water molecules can also diffuse into the materials, potentially altering the device's electrical properties depending on the exposure duration. To investigate this phenomenon, we investigated the bilayer heterojunction device towards 20 ppm of NH_3, under high humidity level (80%) for an extended period of approximately 7 h, at room temperature (20 °C). The quasi-dry sample exhibits a huge drift in baseline current when it exposed to 80% of RH **(Figure S6)**. To focus on transition in the nature of majority charge

carrier and to get a good visibility, we did a baseline correction and divided the single experiment into 4 graphs (labelled as 1 to 4), which are displayed in **Figure S7.**

During the investigation, we witnessed the remarkable transformation on the device's charge transport dynamics. Initially, as expected, the device exhibited n-type behavior, with a gradually diminishing response to NH_3 over time, with an increasing transient effect during the recovery period (**Part 1** of the **Figure S7**). It is indicative of the coexistence of two phenomenon involving charge carriers' density with different kinetics. We can suppose that both surface effect (fast kinetics) and diffusion phenomena (slow kinetics) coexist. During recovery periods, a fascinating kinetic interplay unfolded: an initial sharp decline in current followed by a slower decrease (**Part 2** of the **Figure S7**). Surprisingly, subsequent cycles revealed the reversal process, with the slower decline becoming more pronounced, ultimately shifting the decrease in current entirely to the exposure phase, where a decline in current during NH_3 exposure and an increase during recovery were observed. The n-type device turned to stable p-type behavior, after exposing it to high humidity level (80%) for approximately 210 min.

However, to our surprise, the device underwent another remarkable transformation that was occurred approximately 70 min after the initial transition (t = 280 min). The previously stable p-type behavior began to weaken, marked by a sharp decline in current followed by a sudden increase within the same exposure period (**Part 3** of the **Figure S7**). Consequently, the device undergoes another transition and exhibits again a stable n-type behavior (**Part 4** of the **Figure S7**). Zooming in on the data, we can clearly observe a shift in the dominance of majority charge carriers (holes) over minority charge carriers (electrons) (**Figure 11a**). Around 290 min from the beginning of the experiment, the device displayed a unique equilibrium, where both p- and n-type behaviors occur within the same exposure cycle (**Figure 11b**). This observation underscores the intricate interplay between charge carriers and environmental factors. Anyhow, it is mesmerizing to witness the inversion in device polarity and spectating the changes in nature of majority charge carriers, very closely, which to our knowledge has never reported so far.

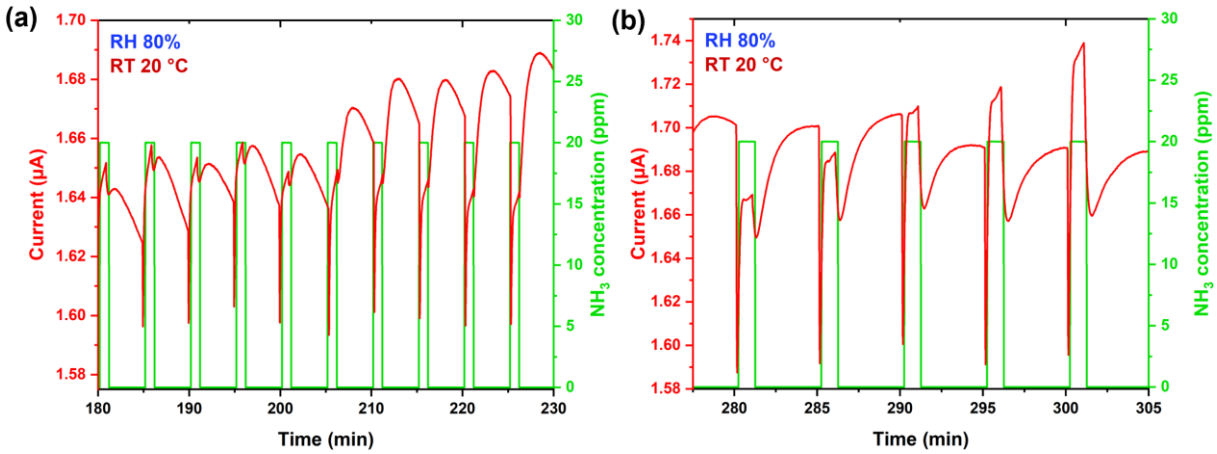

Figure 11. Zoom in the inversion in nature of majority charge carriers from n- to p-type (a) and p- to n-type (b).

Globally, the organic-organic bilayer heterojunction device, with a thickness of 50/50 nm, underwent two distinct episodes of polarity inversion during its ca. 7 h exposure to 80% RH at room temperature. This phenomenon is not only related to the molecular structure of the two components, but also intricately linked to the device's architecture. The initial n-type to p-type transition arises from the gradual diffusion of water into the top layer, altering charge transfer dynamics at the interface by trapping mobile charges that inverse the nature of majority charge carriers in favor of p-type. Subsequent diffusion of water till the interface and into the sublayer affecting the hole mobility, enhancing electron density and leading to the device's transformation into n-type.

Exploring the ambipolarity of the device under oxidating gas species

The stability of the bilayer heterojunction device's ambipolarity was further explored under the influence of strong electron withdrawing species, such as NO_2, across various conditions. Initially, the device underwent exposure to a wide range of humidity levels and gas concentrations, from 80% to 20% RH and from 900 ppb to 300 ppb of NO_2, respectively.

As observed previously in ambient conditions, the device shows p-type behavior (current increases) upon exposure to NO_2. However, it exhibited a decrease in its p-type behavior with decreasing humidity, reflected in the decrease of RR from ca. 25% to 7.5% as humidity declined from 80% to 20% at 900 ppb of NO_2 (**Figure S8**). This phenomenon aligns with our earlier observations and is driven by similar underlying mechanisms. However, contrarily to what happens with NH_3, the response to NO_2 is strongly affected by RH variations.

To delve deeper into achieving ambipolar charge transfer regimes, we investigated the heterojunction device under different temperatures at fixed NO_2 concentration of 200 ppb in a dry environmental condition (RH 10%) (**Figure S9**). To ensure solely effect of the ambipolar

device a freshly prepared sample was utilized. In a dry environment, the device demonstrated observable p-type behavior under NO_2, up to 30 °C. However, as the temperature increased to 40 and 50 °C, the device displayed a diminished response, with no clear polarity observed. Notably, at 60 °C, a significant inversion occurred, transitioning the device to n-type behavior. By utilizing the cooling system, within a few minutes we successfully lowered the temperature back to 30 and 20 °C, where the device returns to the p-type polarity.

Most interestingly, it is the very first report that observes the rather zero state (where the device exhibits no response) of the ambipolar device (at ca. 40 °C) when the domination of majority charge carrier densities goes from p- to n-state or vice versa. For better visibility, the zoom figure was displayed in **Figure S10**. Furthermore, the ambipolar charge transport regime was also achieved at ambient humidity level (RH 45%), by increasing the device temperature from 20 to 80 °C (**Figure 12**).

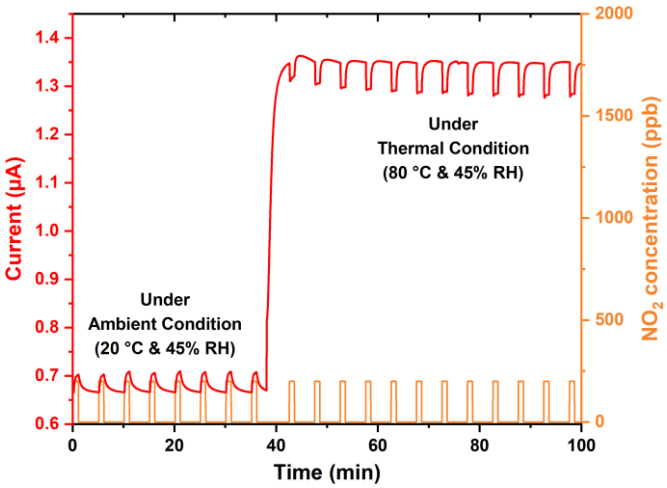

Figure 12. Response curve of $VOF_8Pc/LuPc_2$ heterojunction sensor under exposure of 200 ppb of NO_2 under 20 °C and 80 °C at 45% RH.

As expected, the bilayer heterojunction device exhibits p-type behavior, which shifted to n-type as the temperature raised to 80 °C. Fascinatingly, during first few cycles at 80 °C, the device exhibited a gradually increase in its n-type response, indicating the desorption of water molecules from the solid surface. Subsequently, the device's n-type response rather stabilized, suggesting a dry state and further confirmed the initial state of our ambipolar device. As we discussed earlier, the water molecules can act as a trap for positive mobile charge carriers and their desorption ultimately triggers a detrapping effect, prompting a transformation in the nature of majority charge carriers and resulting in a change in polarity. Additionally, the results aligned well with our previous experimental observations under different conditions. Particularly, it is interesting to compare these results with a previous experiment conducted under same experimental conditions towards 20 ppm of NH_3 exposure (**Figure 7b**). In the previous case,

we observed an amplification in the response at 80 °C compared to ambient conditions, whereas in the current scenario, we observed an inversion in the response.

This type of devices that exhibits ambipolar behavior has the potential to replace two different types of devices (p- and n-type) into a single ambipolar device, eventually reducing the size of the electrical system. Such ambipolar devices hold promise for various applications in nanotechnology, including deployment in spacecraft, satellites, and everyday electrical appliances where minimizing weight and size is crucial. However, achieving precise control over the inversion of majority charge carriers, which determines the device's polarity required a suitable and controllable external trigger, and it may depend on the molecular composition and the architecture of the device. It is crucial to conduct comprehensive investigations into the environmental effects such as humidity and temperature variations when working with ambipolar devices. Moreover, further research is essential before these devices can be effectively deployed in real-world applications. **Table 1** helps us to have a clear view on device's direction of the current change and polarity inversion under NH_3 and NO_2 with respect to the experimental conditions.

Table 1: Comparison of heterojunction device's current change direction and polarity inversion under NH_3 and NO_2 with respect to the experimental conditions. Red upward arrows represent current increase and green downward arrows represent current decrease.

Experimental conditions	Current		Polarity	
	NH_3	NO_2	NH_3	NO_2
10% RH and 20 °C	▲	▲	n-type	p-type
10% RH and 60 °C	▲	▼	n-type	n-type
45% RH and 20 °C	▲	▲	n-type*	p-type
45% RH and 80 °C	▲	▼	n-type	n-type
80% RH and 20 °C	▼	▲	p-type	n-type

*Except if the device has been conditioned in its p-type (long exposure at high humidity value).

Conclusion

We successfully synthesized octafluoro-vanadyl-phthalocyanine (VOF_8Pc) and engaged it as a sublayer in bilayer heterojunction device, combined with lutetium bisphthalocyanine ($LuPc_2$) as a top layer. In current scenario, the charge transport regime of the $VOF_8Pc/LuPc_2$ bilayer heterojunction (ambipolar) device is extensively studied by utilizing different types of external triggers under different gases. The bilayer heterojunction device

demonstrates both p- and n-type behaviors under exposure to oxidation gases (NO_2 and O_3) and reducing gas species (NH_3), depending on humidity levels and temperature variations. The initial polarity of the ambipolar device is identified by observing a current decrease under oxygen exposure, indicates n-type behavior. This is further verified by exposing freshly prepared samples to weak reducing gas (NH_3, current increase) at 20 °C and 45% RH (ambient conditions). Surprisingly, when exposed to strong oxidation gases (NO_2 and O_3) under the same experimental conditions, the device exhibits p-type behavior (current increases) showcasing an ambipolar behavior. However, increasing the temperature of the device to 80 °C revealed its initial n-type polarity even under ambient conditions. Notably, the device exhibits stable response towards NO_2 and NH_3 in both polarity states. Most interestingly, we were capable to observe the zero state where the device exhibits no response (at 40 °C and 10% RH) when the domination of majority charge carrier densities goes from p- to n-state or vice versa. Globally, this type of devices can replace two different types of devices and can be used as a powerful tool in miniature devices, which can dramatically reduce the size of the electrical system.

Supporting Information

The Supporting Information is available free of charge on the ACS Publications website.

Supporting Information contains Raman diffusion spectroscopy, impedance spectroscopy measurements, humidity effect on the nature of majority charge carriers and, NH_3 and NO_2 sensing curves under different experimental conditions.

CRediT authorship contribution statement

Sujithkumar Ganesh Moorthy: Conceptualization, Methodology, Data curation, Formal analysis, Investigation, Writing – original draft, Writing – review & editing. **Adehouyi Apoubou:** Synthesis of VOF_8Pc. **Seydou Ouedraogo:** Supervision, Synthesis of VOF_8Pc, Investigation. **Lucas Vachey:** Performed Impedance measurements. **Mabinty Bayo-Bangoura:** Funding acquisition and Supervision. **Marcel Bouvet:** Funding acquisition, Conceptualization, Methodology, Supervision, Validation, Writing – review & editing.

Notes

The authors declare no competing financial interest.

Acknowledgement

The authors thank CNRS (France) for funding through the ELOCAP project (2021-2023). S. O. is indebted to the Science Institute of Burkina-Faso, for supporting missions in France. We also acknowledge the *Conseil Régional de Bourgogne Franche-Comté* through the Envergure

Program MatElectroCap (2020-2024) and for a Ph. D grant (S. G. M.). The authors acknowledge the *Agence Nationale de la Recherche* for funding through the ANR project Por4Sens, ANR-22-CE06-0039-01. The authors thank the Plateforme d'Analyses Chimiques et de Synthèse Moléculaire de l'Université de Bourgogne (PACSMUB) and the SATT Sayens for technical support in the Raman analyses.

References:

1. Root, S. E.; Savagatrup, S.; Printz, A. D.; Rodriquez, D.; Lipomi, D. J., Mechanical Properties of Organic Semiconductors for Stretchable, Highly Flexible, and Mechanically Robust Electronics. *Chemical Reviews* **2017,** *117* (9), 6467-6499.
2. Wu, Y.; Ma, P.; Wu, N.; Kong, X.; Bouvet, M.; Li, X.; Chen, Y.; Jiang, J., Two-Step Solution-Processed Two-Component Bilayer Phthalocyaninato Copper-Based Heterojunctions with Interesting Ambipolar Organic Transiting and Ethanol-Sensing Properties. *Advanced Materials Interfaces* **2016,** *3* (16), 1600253.
3. Naso, F.; Babudri, F.; Colangiuli, D.; Farinola, G. M.; Quaranta, F.; Rella, R.; Tafuro, R.; Valli, L., Thin Film Construction and Characterization and Gas-Sensing Performances of a Tailored Phenylene−Thienylene Copolymer. *Journal of the American Chemical Society* **2003,** *125* (30), 9055-9061.
4. Povlich, L. K.; Feldman, K. E.; Shim, B. S.; Martin, D. C., 1.130 - Electroactive Polymeric Biomaterials. In *Comprehensive Biomaterials*, Ducheyne, P., Ed. Elsevier: Oxford, 2011; pp 547-561.
5. Wang, M.; Baek, P.; Akbarinejad, A.; Barker, D.; Travas-Sejdic, J., Conjugated polymers and composites for stretchable organic electronics. *Journal of Materials Chemistry C* **2019,** *7* (19), 5534-5552.
6. Bečvář, P.; Krystianiak, A.; Ganesh Moorthy, S.; Jansová, B.; Kohout, M.; Meunier-Prest, R.; Bouvet, M., Electrosynthesized fluorinated polybithiophenes for ammonia sensing. *Materials Chemistry Frontiers* **2024,** *8* (15), 2666-2680.
7. Gong, P.; Yuan, S.; Yu, Z.; Xiao, T.; Li, H.; Ma, S.; Bao, W.; Xu, Z.; Zhou, P.; Zhang, D. W.; Li, Q.; Sun, Z., Long-Range Epitaxial MOF Electronics for Continuous Monitoring of Human Breath Ammonia. *Journal of the American Chemical Society* **2024,** *146* (6), 4036-4044.
8. Zhou, Y.; Han, S.-T., *Ambipolar Materials and Devices*. The Royal Society of Chemistry: 2020.
9. Ouedraogo, S.; Meunier-Prest, R.; Kumar, A.; Bayo-Bangoura, M.; Bouvet, M., Modulating the Electrical Properties of Organic Heterojunction Devices Based On Phthalocyanines for Ambipolar Sensors. *ACS Sensors* **2020,** *5* (6), 1849-1857.
10. Ganesh Moorthy, S.; Ouedraogo, S.; Bouvet, M., Ambipolar Heterojunction Sensors: Another Way to Detect Polluting Gases. *ACS Sensors* **2024,** *9* (7), 3707-3719.
11. Kong, X.; Tarakanova, E. N.; Du, X.; Tomilova, L. G.; Chen, Y., Discrimination and detection of NO2, NH3 and H2S using sensor array based on three ambipolar sandwich tetradiazepinoporphyrazinato/phthalocyaninato europium double-decker complexes. *Materials Advances* **2023,** *4* (6), 1515-1522.
12. Wang, Y.; Liao, Q.; She, D.; Lv, Z.; Gong, Y.; Ding, G.; Ye, W.; Chen, J.; Xiong, Z.; Wang, G.; Zhou, Y.; Han, S.-T., Modulation of Binary Neuroplasticity in a Heterojunction-Based Ambipolar Transistor. *ACS Applied Materials & Interfaces* **2020,** *12* (13), 15370-15379.
13. Zaumseil, J.; Sirringhaus, H., Electron and Ambipolar Transport in Organic Field-Effect Transistors. *Chemical Reviews* **2007,** *107* (4), 1296-1323.
14. Bouvet, M.; Ouedraogo, S.; Meunier-Prest, R., Ambipolar Materials for Gas Sensing. In *Ambipolar Materials and Devices*, Zhou, Y.; Han, S.-T., Eds. The Royal Society of Chemistry: 2020; p 446.
15. Guillaud, G.; Al Sadoun, M.; Maitrot, M.; Simon, J.; Bouvet, M., Field-effect transistors based on intrinsic molecular semiconductors. *Chemical Physics Letters* **1990,** *167* (6), 503-506.
16. Dutta, S.; Lewis, S. D.; Dodabalapur, A., Hybrid organic/inorganic ambipolar thin film transistor chemical sensor. *Applied Physics Letters* **2011,** *98* (21), 213504.

17. Bouvet, M.; Parra, V., Semiconductor transducer, and its use in a sensor for detecting electron donor or electron acceptor species, Patent US8450725 B2, 2013.
18. Kumar, A.; Nwosu, I. D.; Meunier-Prest, R.; Lesniewska, E.; Bouvet, M., Tuning of Interfacial Charge Transport in Organic Heterostructures via Aryl Electrografting for Efficient Gas Sensors. *ACS Applied Materials & Interfaces* **2024,** *16* (3), 3795-3808.
19. Ganesh Moorthy, S.; Arvidson, J.; Meunier-Prest, R.; Wang, H.; Bouvet, M., π-Extended Porphyrin–Phthalocyanine Heterojunction Devices Exhibiting High Ammonia Sensitivity with a Remarkable Light Effect. *ACS Sensors* **2024,** *9* (2), 883-894.
20. Clarisse, C.; Riou, M. T., Synthesis and characterization of some lanthanide phthalocyanines. *Inorganica Chimica Acta* **1987,** *130* (1), 139-144.
21. King, B.; Ganesh Moorthy, S.; Lesniewska, E.; Meunier-Prest, R.; Bouvet, M.; Lessard, B. H., Modulating the majority charge carrier type and performance of organic heterojunction ammonia sensors by increasing peripheral fluorination of the silicon phthalocyanine sublayer. *Sensors and Actuators B: Chemical* **2024,** *408*, 135507.
22. Loma Kikobo, G.; Kumar, A.; Vibhu, V.; Ouedraogo, S.; Deshotel, A.; Mateos, M.; Meunier-Prest, R.; Bouvet, M., Photon assisted-inversion of majority charge carriers in molecular semiconductor-based organic heterojunctions. *Journal of Materials Chemistry C* **2021,** *9* (14), 5008-5020.
23. Sukhikh, A.; Klyamer, D.; Bonegardt, D.; Basova, T., Octafluoro-Substituted Phthalocyanines of Zinc, Cobalt, and Vanadyl: Single Crystal Structure, Spectral Study and Oriented Thin Films. *International Journal of Molecular Sciences* **2023,** *24* (3), 2034.
24. VanCott, T. C.; Gasyna, Z.; Schatz, P. N.; Boyle, M. E., Magnetic circular dichroism and absorption spectra of lutetium bis(phthalocyanine) isolated in an argon matrix. *The Journal of Physical Chemistry* **1995,** *99* (13), 4820-4830.
25. Ortí, E.; Brédas, J. L.; Clarisse, C., Electronic Structure of Phthalocyanines: Theoretical Investigation of the Optical Properties of Phthalocyanine Monomers, Dimers, and Crystals. *The Journal of Chemical Physics* **1990,** *92* (2), 1228.
26. Ouedraogo, S.; Coulibaly, T.; Meunier-Prest, R.; Bayo-Bangoura, M.; Bouvet, M., p-Type and n-type conductometric behaviors of octachloro-metallophthalocyanine-based heterojunctions, the key role of the metal. *Journal of Porphyrins and Phthalocyanines* **2020,** *24*, 750-757.
27. Ganesh Moorthy, S.; King, B.; Kumar, A.; Lesniewska, E.; Lessard, B. H.; Bouvet, M., Molecular Engineering of Silicon Phthalocyanine to Improve the Charge Transport and Ammonia Sensing Properties of Organic Heterojunction Gas Sensors. *Advanced Sensor Research* **2022,** *2* (3), 2200030.
28. Di Zazzo, L.; Ganesh Moorthy, S.; Meunier-Prest, R.; Lesniewska, E.; Di Natale, C.; Paolesse, R.; Bouvet, M., Ammonia and Humidity Sensing by Phthalocyanine–Corrole Complex Heterostructure Devices. *Sensors* **2023,** *23* (15), 6773.
29. Liu, S.; Wang, H.; Wang, X.; Li, S.; Liu, H.; Chen, Y.; Li, X., Diverse sensor responses from two functionalized tris(phthalocyaninato)europium ambipolar semiconductors towards three oxidative and reductive gases. *Journal of Materials Chemistry C* **2019,** *7* (2), 424-433.
30. Ganesh Moorthy, S.; Bouvet, M., Effects of Visible Light on Gas Sensors: From Inorganic Resistors to Molecular Material-Based Heterojunctions. *Sensors* **2024,** *24* (5), 1571.
31. Bouvet, M.; Mateos, M.; Wannebroucq, A.; Navarrete, E.; Llobet, E., A tungsten oxide–lutetium bisphthalocyanine n–p–n heterojunction: from nanomaterials to a new transducer for chemo-sensing. *Journal of Materials Chemistry C* **2019,** *7* (21), 6448-6455.
32. Kumar, A.; Meunier-Prest, R.; Lesniewska, E.; Bouvet, M., Interplay of electrode geometry and bias on charge transport in organic heterojunction gas sensors. *Sensors and Actuators B: Chemical* **2022,** *369*, 132313.
33. Wannebroucq, A.; Ouedraogo, S.; Meunier-Prest, R.; Suisse, J.-M.; Bayo, M.; Bouvet, M., On the interest of ambipolar materials for gas sensing. *Sensors and Actuators B: Chemical* **2018,** *258*, 657-664.
34. Asay, D. B.; Kim, S. H., Evolution of the Adsorbed Water Layer Structure on Silicon Oxide at Room Temperature. *The Journal of Physical Chemistry B* **2005,** *109* (35), 16760-16763.
35. Matsuguchi, M.; Okamoto, A.; Sakai, Y., Effect of humidity on NH3 gas sensitivity of polyaniline blend films. *Sensors and Actuators B: Chemical* **2003,** *94* (1), 46-52.